B Article Submitted for Publication on the Astrophysical Journal

THE EFFECTS OF DIFFERENTIAL ROTATION ON THE MAGNETIC STRUCTURE OF THE SOLAR CORONA: MHD SIMULATIONS

Roberto Lionello, Pete Riley, Jon A. Linker, and Zoran Mikić

Science Applications International Corporation, San Diego, CA 92121-1578

{lionellor,rileype,linkerj,mikicz}@saic.com

Received _____; accepted _____

ABSTRACT

Coronal holes are magnetically open regions from which the solar wind streams. Magnetic reconnection has been invoked to reconcile the apparently rigid rotation of coronal holes with the differential rotation of magnetic flux in the photosphere. This mechanism might also be relevant to the formation of the slow solar wind, the properties of which seem to indicate an origin from the opening of closed magnetic field lines. We have developed a global MHD model to study the effect of differential rotation on the coronal magnetic field. Starting from a magnetic flux distribution similar to that of Wang et al. (1996), which consists of a bipolar magnetic region added to a background dipole field, we applied differential rotation over a period of 5 solar rotations. The evolution of the magnetic field and of the boundaries of coronal holes are in substantial agreement with the findings of Wang et al.. We identified examples of interchange reconnection and other changes of topology of the magnetic field. Possible consequences for the origin of the slow solar wind are also discussed.

Subject headings: MHD — solar wind — Sun: corona — Sun: magnetic fields — Sun: activity

1. INTRODUCTION

Although the details of the solar rotation rate are quite difficult to measure, sunspot drawings long ago revealed that low-latitude spots rotated considerably faster than those at higher latitudes (Zirin 1988, p. 115). Newton & Nunn (1951) found that the Sun's equator rotates 17% faster than the poles. Subsequent observations (Timothy et al. 1975; Adams & Tang 1977; Tang 1981; Snodgrass 1983; Howard et al. 1983) differed slightly on the observed differential rotation profile but confirmed the slower rotation of high latitude regions.

Coronal holes are extended regions of open magnetic field (Altschuler et al. 1972; Levine et al. 1977; Pneuman et al. 1978) with densities significantly lower than the typical background corona (Munro & Withbroe 1972; Withbroe & Wang 1972). For this reason they appear darker in X-ray and extreme-ultraviolet emission and brighter in He I 10830 Å absorption. The properties of coronal holes derived from the Skylab mission were summarized in Bohlin (1976) and Bohlin (1976). Rather surprisingly, the Skylab mission found a coronal hole that appeared to rotate more like a solid body than differentially, with only a 3% variation in rotational velocity between pole and equator (Timothy et al. 1975).

An explanation for these seemingly contradictory phenomena was proposed by Wang et al. (1996). They assumed an idealized photospheric magnetic flux distribution consisting of a dipole plus a bipolar magnetic region located predominantly in the southern hemisphere but extending across the equator. By evolving the photospheric field in response to differential rotation, and calculating the instantaneous coronal magnetic field using a source-surface (i.e. current-free) model, they found that the presence of the bipolar magnetic region breaks the symmetry of the dipole and that the polar coronal holes develop extensions reaching towards the equator. According to Wang et al. (1996), the northern hemisphere extension appeared to rotate almost rigidly. The apparent rigid rotation of coronal holes, when coupled with the differential rotation of magnetic flux elements in the photosphere, implies that the footpoints of magnetic field lines

are convected across the boundaries of coronal holes. From this follows that magnetic field lines alternatively open up (when entering a coronal hole) or close down (when exiting), which led Wang et al. to conclude that magnetic reconnection is necessary to rearrange the coronal magnetic field.

Fisk et al. (1999) pointed out that the model of Wang et al. (1996) is intrinsically static, since the field configuration is determined from a potential field model. In a series of articles, Fisk (1996), Fisk et al. (1998), Fisk et al. (1999), and Fisk (2001) presented a complementary explanation, which is referred to as the Fisk model. Fisk et al. (1999) assume that the magnetic field in the corona is essentially radial and in magnetic pressure equilibrium. However the magnetic field lines are anchored to a differentially rotating photosphere. As a consequence, magnetic field lines in the corona are moved across coronal holes until they encounter low-latitude loops and reconnect with them.

The Ulysses probe (Phillips et al. 1995) found that the solar wind consists of two streams with distinct properties: a fast solar wind that originates from polar coronal holes, having an almost steady speed of ~ 750 km s^{-1}, and a slow solar wind with a more variable speed averaging about 400 km s^{-1}. Observations by Ulysses (McComas et al. 1998), UVCS (Noci et al. 1997; Habbal et al. 1997; Strachan et al. 2002), LASCO (Sheeley et al. 1997; Tappin et al. 1999; Lewis & Simnett 2000, 2002), and Doppler scintillation (Woo & Gazis 1994) have associated the slow solar wind with dense equatorial regions and streamer belts. The slow solar wind is enhanced in elements with low first ionization potential (Geiss et al. 1995; Wimmer-Schweingruber et al. 1997; Zurbuchen et al. 1999, 2002; Pagel et al. 2004), a phenomenon also observed in coronal loops (Feldman & Widing 1993; Feldman et al. 1998). Therefore both Wang et al. (1996) and Fisk et al. (1998) argued that the slow solar wind may originate from the opening of coronal loops reconnecting with open field lines. It has also been found that *in situ* measurements of the slow solar wind can be traced back to the boundaries of coronal holes (Neugebauer et al. 1998;

Linker et al. 1999; Neugebauer et al. 2002; Riley et al. 2003), where the reconnection between closed loops and open field lines is presumed to occur. However, these inferences of the sources of the slow solar wind were unable to address the details of this reconnective process. A different mechanism to account for the origin of the slow solar wind has been proposed by Einaudi et al. (1999, 2000), who explained the properties of the wind through an instability in the current sheet above helmet streamers. The three-fluid numerical MHD model of Ofman (2000, 2004) used a heating function constrained by observations to reproduce the properties of the slow solar wind, including the enhanced emission in the O^5+ line in SOHO/UVCS observations.

In this study, we apply our 3-D, time-dependent MHD model (Mikić et al. 1999) to study the changes in the coronal magnetic field in response to differential rotation at the photosphere, and to investigate what these changes imply for the origin of the slow solar wind and the properties of the heliosphere. In § 2 we describe our model, the initial conditions, the boundary conditions, and how we have incorporated differential rotation. In § 3 we present our results, and in § 4 we discuss the implications of this study.

2. MODEL DESCRIPTION

To study the effect of differential rotation on the magnetic structure of the corona, we use the MHD approximation, which correctly reproduces long-scale, low-frequency phenomena in magnetized plasmas such as the solar corona. Our model uses spherical coordinates and advances in time the following set of viscous and resistive MHD equations:

$$\nabla \times \mathbf{B} = \frac{4\pi}{c}\mathbf{J}, \tag{1}$$

$$\nabla \times \mathbf{E} = -\frac{1}{c}\frac{\partial \mathbf{B}}{\partial t}, \tag{2}$$

$$\mathbf{E} + \frac{\mathbf{v} \times \mathbf{B}}{c} = \eta \mathbf{J}, \tag{3}$$

$$\frac{\partial \rho}{\partial t} + \nabla \cdot (\rho \mathbf{v}) = 0, \tag{4}$$

$$\frac{1}{\gamma-1}\left(\frac{\partial T}{\partial t}+\mathbf{v}\cdot\nabla T\right) = -T\nabla\cdot\mathbf{v}, \quad (5)$$

$$\rho\left(\frac{\partial \mathbf{v}}{\partial t}+\mathbf{v}\cdot\nabla\mathbf{v}\right) = \frac{1}{c}\mathbf{J}\times\mathbf{B}-\nabla p+\rho\mathbf{g}+\nabla\cdot(\nu\rho\nabla\mathbf{v}), \quad (6)$$

where $\mathbf{B}$ is the magnetic field, $\mathbf{J}$ is the electric current density, $\mathbf{E}$ is the electric field, ρ, $\mathbf{v}$, p, and T are the plasma mass density, velocity, pressure, and temperature. $\mathbf{g}=-g_0\hat{\mathbf{r}}/r^2$ is the gravitational acceleration, η the resistivity, ν is the kinematic viscosity. $\gamma = 1.05$ is the polytropic index. This approximation can be justified for the present study, since we are modeling the magnetic configuration of the corona and not the detailed properties of the plasma such as the contrast in temperature and density between closed and open field regions, or the contrast in speed between fast and slow wind, for which a more sophisticated model would be necessary (Lionello et al. 2001).

On the solar surface we prescribe a magnetic flux distribution similar to that of Wang et al. (1996), consisting of a dipole field with 1 G intensity at the poles plus a bipolar "active region":

$$\begin{aligned} B_r(\theta,\phi) &= \cos\theta-\frac{10}{b_w}\exp\left(-\frac{(\theta-\theta_0)^2}{2b_w^2}-\frac{(\phi-\phi_1)^2}{2b_w^2}\right) \\ &\quad +\frac{10}{b_w}\exp\left(-\frac{(\theta-\theta_0)^2}{2b_w^2}-\frac{(\phi-\phi_2)^2}{2b_w^2}\right), \\ &\quad \theta_0=\frac{7}{12}\pi,\quad \phi_1=\frac{5}{6}\pi,\quad \phi_2=\frac{7}{6}\pi,\quad b_w=0.3. \end{aligned} \quad (7)$$

To model differential rotation, Wang et al. (1996) prescribed angular velocity on the solar surface according to

$$\omega(\theta)=13.39-2.77\cos^2\theta \text{ degrees day}^{-1}, \quad (8)$$

We have prescribed:

$$\omega(\theta)=-27.7\cos^2\theta \text{ degrees day}^{-1}. \quad (9)$$

The differential rotation factor is ten times larger and the overall rigid rotation rate of the Sun has been neglected. This has been done to speed up the physical effects of the differential flow

and obtain results in a reasonable amount of computer time. This approximation can be justified considering that the magnitude of the tangential velocity associated with differential rotation is still far below the Alfvén and sound speeds in the corona (Lionello et al. 2001). Neglecting the rigid rotation rate of the Sun is equivalent to computing in the corotating frame, but dropping noninertial terms, which are small in the corona. At the inner radial boundary the component of the velocity along the magnetic field is calculated from the characteristic equations. A fixed temperature of 1.8×10^6 K and an electron density of 10^8 cm^{-3} are also prescribed at the inner boundary. At the outer radial boundary the flow is supersonic and super-Alfvénic. The calculation described here has been performed on a $61 \times 71 \times 64$ nonuniform (r, θ, ϕ) grid, with $\Delta r \approx 1.8 \times 10^{-2}\ R_\odot = 12$ Mm at the lower radial boundary and $\Delta r \approx 3.1\ R_\odot$ at $30\ R_\odot$; $\Delta\theta$ varies between $\Delta\theta \approx 3.5°$ at the poles and $\Delta\theta \approx 1.9°$ near the equator. The azimuthal mesh is uniform. The simulation domain extends out to $30 R_\odot$. A uniform resistivity η has been used, corresponding to a resistive diffusion time $\tau_R = \frac{4\pi R_\odot^2}{\eta c^2} = 1.6 \times 10^4$ hours. At the pole, where $|\mathbf{B}| = 1$ G and $n_0 = 10^8$ cm^{-3}, the Alfvén speed is $V_A = 218$ km/s and the Alfvén travel time at the base of the corona is $\tau_A = R_\odot / V_A = 53$ minutes. At the center of the active region poles, $V_A = 559$ km/s. A uniform viscosity ν is also used, corresponding to a viscous diffusion time $\tau_\nu = \frac{R_\odot^2}{\nu} = 40$ hours. These values of resistivity and viscosity are much larger than the solar values and are used to dissipate unresolved structures that would be smaller than the grid resolution. The upwinding treatment of advection introduces numerical dissipation beyond the values specified explicitly above (Lionello et al. 1998). Under the streamer, where the flow is almost absent, numerical dissipation is a small fraction of the prescribed resistivity and viscosity and does not play a significant role. It becomes comparable with the prescribed viscosity at about 2 solar radii. Further out the mesh size and the flow are large and numerical dissipation greatly exceeds the specified resistivity and viscosity. We have found that solutions with smaller values of viscosity and resistivity have somewhat smaller closed-field regions and larger magnetic energies. However the solutions are qualitatively similar.

The simulation was initiated with a spherically symmetric transonic Parker solar wind solution and a potential magnetic field corresponding to the flux distribution of Eq. (7). After a relaxation period of 64.5 hours, during which the initial field relaxed to configuration with a streamer and a current sheet, we started differential rotation according to Eq. (9). We integrated the equations for 322.6 hours. Since the differential rotation rate in Eq. (9) is ten times the solar amount, the shear introduced during the integration time is equivalent to that of 3226 hours, i.e. 5 solar rotations (similar to Wang et al. (1996)). Henceforward we will measure time in terms of fractional solar rotations, keeping in mind that for us one solar rotation is actually 64.5 hours.

3. RESULTS

The most dramatic effect of differential rotation is the distortion of the magnetic flux distribution on the solar surface. Figure 1 shows projections of B_r taken at intervals of 0.625 solar rotation. During the simulation, the shape of the active region becomes increasingly distorted as more and more shear is introduced by the surface flow of Eq. (9). Its effect is more evident at higher latitudes.

Since we know the magnetic field in the computational domain at each instant in time, we can produce a "coronal-hole" map by tracing magnetic field lines from the solar surface. We can distinguish between regions of open magnetic flux, which we define as coronal holes, and the regions of closed magnetic flux. In Fig. 2 we show the evolution of coronal-hole boundaries at the same times as Fig. 1. Dark grey represents closed-field regions, while light gray indicates coronal holes. Notice that the extension of the northern coronal hole remains relatively unchanged during five solar rotations (indicating rigid rotation and in agreement with Skylab observations), while the southern coronal hole is considerably distorted. We also plot the launch points of several magnetic field lines. These footpoints are advected by the shearing flow of Eq. (9) and enter and exit the regions of closed or open flux. We have color coded them to show how an initially

open (closed) line is successively closed (opened), sometimes multiple times, through magnetic reconnection as it crosses the coronal-hole boundaries that remain relatively unchanged in the northern hemisphere. Footpoints of open field lines are black. If they reconnect and close down the color of their footpoints is changed to green. If these field lines open up again they are marked cyan. Moreover, if they close down for a second time their color is changed to yellow. One of these points has been encircled to allow the reader to better follow its evolution: it moves inside a closed field region in the third frame and subsequently reenters the southern polar coronal hole (in the eight frame). Red footpoints indicate field lines that are (and initially were) closed. The color of these footpoints is changed to blue if the corresponding field line opens up. A box encloses one of these points as it moves along its path on the solar surface and opens up when it enters the northern coronal hole in the fifth frame. The successive opening and closing of these magnetic field lines can be clearly seen in Fig. 3, where we present a view from a distance of 5 $R_\odot$ from the solar surface. As the footpoints are advected, red field lines become elongated and open up into the solar wind, while black field lines close down to form green loops, and so on.

Figure 4 is a schematic showing the three types of magnetic field line evolution we have identified during the simulation. In Fig. 4(a) we show a closed loop that expands and opens out into the solar wind. Figure 4(b) illustrates the reconnection of two open field lines to form a disconnected loop. In Fig. 4(c) the reconnection of a closed loop with an open field line is shown: this event has been dubbed "interchange reconnection" (Crooker et al. 2002). Representative events of these three types of magnetic reconnection are presented in Figure 5. In the two frames of Fig. 5(a), which are taken at an interval of $t_2 - t_1 = 0.0625$ solar rotation, we show an event of the first type: magnetic field lines forming a loop are stretched out and eventually open up into the corona. This event should be compared with Fig. 4(a). We have no way to tell whether these field lines have indeed opened or they merely close beyond our computational domain. In Fig. 5(b) we show open magnetic field lines in an X-shaped configuration that close down to form a streamer and a disconnected loop as in Fig. 4(b) (since the disconnected loop is quickly carried away in

the solar wind, we were not able to identify and plot it). Finally, an example of interchange reconnection as in Fig. 4(c) is shown in Fig. 5(c), which involves a loop and an open magnetic flux tube that is dragged towards the former. The original loop is opened up and a new loop is formed.

To understand where the field lines undergoing reconnection are rooted on the solar surface, we compared two coronal hole maps, one at $t = t_1$ and the other at $t = t_2$. For each point $\mathbf{x}_2 = [\theta, \phi(t_2)]$ on the solar surface we calculated

$$\mathbf{x}_1 = [\theta, \phi(t_1)] = [\theta, \phi(t_2) - \omega(\theta)(t_2 - t_1)]. \tag{10}$$

Figure 6 shows a projection of the solar surface at $t = t_2$ that was color-coded to emphasize changes in connectivity: if both $\mathbf{x}_2$ and $\mathbf{x}_1$ give rise to open field lines then $\mathbf{x}_2$ is light grey. If the field line remains closed, the color is dark grey. Red indicates regions where the field lines have just closed down to form a loop. In contrast, the magnetic flux in blue areas, which was previously closed, has just opened up. The areas of changing connectivity (red and blue) are all found at the boundaries between flux that does not change connectivity i.e., at the boundaries of coronal holes. Although there are exceptions, blue areas appear to be more frequent on the eastward boundaries of coronal holes, while red areas are more frequent on the westward boundaries. In particular the blue areas are the most likely candidates for the sources of the slow solar wind, which originates from the opening of closed magnetic structures according to both Wang et al. (1996) and Fisk et al. (1998).

A different point of view of the reconnection process is presented in Fig. 7. This figure shows maps of the connectivity of magnetic field lines at 30 $R_\odot$. The larger fraction of the heliosphere at 30 $R_\odot$ is occupied by open magnetic flux connected to the solar surface (dark grey areas). Only the region surrounding the current sheet (white) is occupied by field lines that are not connected to the Sun but have both end points on the $r = 30\ R_\odot$ surface. These are transient features and, provided they are truly disconnected, they can be associated with reconnection events of the type shown in Fig. 5(b), which involve the outward propagation of material that was formerly trapped

in closed magnetic field lines into the solar wind. However, since 30 $R_\odot$ is the upper limit of our computational domain, we cannot exclude the possibility that these U-shaped lines might not be dips of field lines otherwise connected through one or both ends to the solar surface. An interchange reconnection event as that of Fig. 5(c) may form field lines with one end anchored to the photosphere and with dips advected into the solar wind (the dashed line in the figure indicates the outer boundary).

4. SUMMARY AND DISCUSSION

We have presented a simulation to investigate the effects of differential rotation at the solar surface and its manifestation in the dynamic evolution of the magnetic structure of the corona. We have shown how the magnetic flux distribution is sheared by differential rotation flow, while the coronal hole boundaries may remain relatively unchanged. Magnetic field lines enter and exit the coronal hole boundary and undergo magnetic reconnection. We have shown how and where this reconnection occurs and what its implication is for the origin of the slow solar wind.

Our investigation was modeled after Wang et al. (1996) and our results are in agreement with theirs, lending support to the use of Potential-Field Source-Surface models to study such phenomena. Coronal hole extensions are formed when magnetic regions are present beside the solar dipole. Therefore the evolution of coronal holes is dependent on that of the flux of the magnetic regions from which they originate. The origin and evolution of the northern coronal hole extension is tied to the low-latitude portion of the active region. Since differential rotation is negligible around the equator, this part of magnetic flux does not evolve appreciably and the northern coronal hole extension shows relatively small changes. On the contrary, the southern coronal hole extension, which is tied to that part of of the active region that evolves considerably, is subject to noticeable distortion. Parcels of plasma are convected by the differential flow at the solar surface; the field lines rooted in these parcels either close down onto the Sun or open up into

the solar wind as they exit or enter the coronal holes.

In our simulations we distinguished between three general types of reconnection events: magnetic loops that are opened up into the solar wind, closing down of open field lines, and interchange reconnection between loops and open flux tubes (Crooker et al. 2002). We can link these types of events with *in situ* observations of the solar wind (e.g. Gosling et al. 2002; Crooker et al. 2004). Both open flux from inside coronal holes and those field lines that originate through interchange reconnection are characterized by the presence of a unidirectional heat flux coming from the Sun. Bidirectional heat flux is also observed sometimes and can be often associated with plasma that is part of closed field structures that are being dragged out by the solar wind. The absence of heat flux is rare and can be associated with disconnected magnetic field lines. The frequency and distribution of these events may have been affected by our choice of parameters, as discussed below.

We have identified regions where closed magnetic loops undergo reconnection and release their contents into the solar wind. This occurs at the boundary regions of coronal holes, as pointed out by Wang & Sheeley (1990). From our model it appears that these areas are not uniformly distributed but tend to concentrate on the eastward borders of closed field regions. This prediction from our model can be tested by comparison with solar wind *in situ* observations mapped back to the solar surface. The plasma in the loops, which are about to open up, is enriched in elements with a low first ionization potential (Zurbuchen et al. 1998), a characteristic property of the slow solar wind. Moreover, the readily opened field lines at the boundary of coronal holes have large expansion factors leading to slower solar wind flow (Wang et al. 1996; Arge et al. 2003). The interchange reconnection mechanism, described by Fisk et al. (1998), may be responsible for the release of plasma. However, it is also possible that the shearing of loops can open them. Interchange reconnection between open and closed field lines might become the primary mechanism to release the slow solar wind when parasitic polarities are introduced into the model.

We intend to repeat the calculation with a more realistic magnetic flux distribution to determine its effect on the reconnection process and the fraction of field lines that continuously open up to the solar wind.

Given the number of approximations that we have introduced (out of numerical necessity), it is reasonable to ask how realistic our model is. First, the polytropic approximation can be justified when one is interested in modeling the magnetic structure and not the plasma properties of the solar wind. Second, in modeling differential rotation we neglected the overall rotation of the Sun and speeded up the differential flow by a factor 10. Although the speed of the flow is still well below the Alfvén and sound speeds, this has a qualitative effect on the details of the magnetic processes. Higher flow speeds cause loops to increase in height more rapidly before undergoing reconnection. Therefore the event pictured in Fig. 5(c) would probably have occurred at lower heights, had a more realistic value of the solar differential flow been used. Moreover, disconnected field lines in the heliosphere (Fig. 7), i.e. plasmoids, produced by some reconnection events in the lower corona, would have been confined to the vicinity of the current sheet and their frequency would probably have been lower. To verify our conclusions we repeated part of the simulation with a differential flow that was only 5 times larger than the solar value and obtained results in qualitative agreement. Third, our flux distribution is very simplified in comparison to a magnetogram. In particular, it does not include parasitic polarities. In addition the "active region" is unrealistically large. The introduction of parasitic polarities may create small scale loops, with which the open magnetic flux tube could have undergone interchange reconnection as suggested by Fisk et al. (1998), instead of reconnecting with another open magnetic tube.

In this paper we have not addressed the heliospheric consequences of differential rotation. For example, Forsyth et al. (1995) found the heliospheric magnetic field to be under-wound at low heliographic latitudes. Fisk (1996) explained this as a consequence of differential rotation, which under the right circumstances, could lead to field line motion in a direction opposite to the rotation

of the Sun. By introducing a more realistic value for differential rotation, including the overall rotation of the Sun, and modeling out to 5 AU, it should be possible to explore this mechanism in more detail. We intend to do that in future investigations.

This work was supported by NASA's Support Research and Technology and Sun-Earth Connection Theory programs PR would like to acknowledge support from NASA SEG-GI (S-54538-G) and SR&T (NASW-03013) contracts.

REFERENCES

Adams, W. M., & Tang, F. 1977, Sol. Phys., 55, 499

Altschuler, M. D., Trotter, D. E., & Orrall, F. Q. 1972, Sol. Phys., 26, 354

Arge, C. N., Odstrcil, D., Pizzo, V. J., & Mayer, L. R. 2003, in AIP Conf. Proc. 679: Solar Wind Ten, 190–193

Bohlin, J. D. 1976, in Physics of Solar Planetary Environments, 114–128

Crooker, N. U., Forsyth, R., Rees, A., Gosling, J. T., & Kahler, S. W. 2004, Journal of Geophysical Research (Space Physics), 6110

Crooker, N. U., Gosling, J. T., & Kahler, S. W. 2002, Journal of Geophysical Research (Space Physics), 107, 3

Einaudi, G., Boncinelli, P., Dahlburg, R. B., & Karpen, J. T. 1999, J. Geophys. Res., 104, 521

—. 2000, Advances in Space Research, 25, 1931

Feldman, U., Schühle, U., Widing, K. G., & Laming, J. M. 1998, ApJ, 505, 999

Feldman, U., & Widing, K. G. 1993, ApJ, 414, 381

Fisk, L. A. 1996, J. Geophys. Res., 101, 15547

—. 2001, J. Geophys. Res., 106, 15849

Fisk, L. A., Schwadron, N. A., & Zurbuchen, T. H. 1998, Space Science Reviews, 86, 51

Fisk, L. A., Zurbuchen, T. H., & Schwadron, N. A. 1999, ApJ, 521, 868

Forsyth, R. J., Balogh, A., Smith, E. J., Murphy, N., & McComas, D. J. 1995, Geophys. Res. Lett., 22, 3321

Geiss, J., Gloeckler, G., & von Steiger, R. 1995, Space Science Reviews, 72, 49

Gosling, J. T., Skoug, R. M., Feldman, W. C., & McComas, D. J. 2002, Geophys. Res. Lett., 29, 14

Habbal, S. R., Woo, R., Fineschi, S., O'Neal, R., Kohl, J., Noci, G., & Korendyke, C. 1997, ApJ, 489, L103+

Howard, R., Adkins, J. M., Boyden, J. E., Cragg, T. A., Gregory, T. S., Labonte, B. J., Padilla, S. P., & Webster, L. 1983, Sol. Phys., 83, 321

Levine, R. H., Altschuler, M. D., Harvey, J. W., & Jackson, B. V. 1977, ApJ, 215, 636

Lewis, D. J., & Simnett, G. M. 2000, MNRAS, 317, 1005

—. 2002, MNRAS, 333, 969

Linker, J. A., Mikić, Z., Biesecker, D. A., Forsyth, R. J., Gibson, S. E., Lazarus, A. J., Lecinski, A., Riley, P., Szabo, A., & Thompson, B. J. 1999, J. Geophys. Res., 104, 9809

Lionello, R., Linker, J. A., & Mikić, Z. 2001, ApJ, 546, 542

Lionello, R., Mikić, Z., & Schnack, D. D. 1998, Journal of Computational Physics, 140, 1

McComas, D. J., Bame, S. J., Barraclough, B. L., Feldman, W. C., Funsten, H. O., Gosling, J. T., Riley, P., Skoug, R., Balogh, A., Forsyth, R., Goldstein, B. E., & Neugebauer, M. 1998, Geophys. Res. Lett., 25, 1

Mikić, Z., Linker, J. A., Schnack, D. D., Lionello, R., & Tarditi, A. 1999, Phys. of Plasmas, 6, 2217

Munro, R. H., & Withbroe, G. L. 1972, ApJ, 176, 511

Neugebauer, M., Forsyth, R. J., Galvin, A. B., Harvey, K. L., Hoeksema, J. T., Lazarus, A. J., Lepping, R. P., Linker, J. A., Mikić, Z., Steinberg, J. T., von Steiger, R., Wang, Y.-M., & Wimmer-Schweingruber, R. F. 1998, J. Geophys. Res., 103, 14587

Neugebauer, M., Liewer, P. C., Smith, E. J., Skoug, R. M., & Zurbuchen, T. H. 2002, Journal of Geophysical Research (Space Physics), 107, 13

Newton, H. W., & Nunn, M. L. 1951, MNRAS, 111, 413

Noci, G., Kohl, J. L., Antonucci, E., Tondello, G., Huber, M. C. E., Fineschi, S., Gardner, L. D., Korendyke, C. M., Nicolosi, P., Romoli, M., Spadaro, D., Maccari, L., Raymond, J. C., Siegmund, O. H. W., Benna, C., Ciaravella, A., Giordano, S., Michels, J., Modigliani, A., Naletto, G., Panasyuk, A., Pernechele, C., Poletto, G., Smith, P. L., & Strachan, L. 1997, in ESA SP-404: Fifth SOHO Workshop: The Corona and Solar Wind Near Minimum Activity, 75

Ofman, L. 2000, Geophys. Res. Lett., 27, 2885

—. 2004, Advances in Space Research, 33, 681

Pagel, A. C., Crooker, N. U., Zurbuchen, T. H., & Gosling, J. T. 2004, Journal of Geophysical Research (Space Physics), 1113

Phillips, J. L., Bame, S. J., Barnes, A., Barraclough, B. L., Feldman, W. C., Goldstein, B. E., Gosling, J. T., Hoogeveen, G. W., McComas, D. J., Neugebauer, M., & Suess, S. T. 1995, Geophys. Res. Lett., 22, 3301

Pneuman, G. W., Hansen, S. F., & Hansen, R. T. 1978, Sol. Phys., 59, 313

Riley, P., Mikić, Z., Linker, J., & Zurbuchen, T. H. 2003, in AIP Conf. Proc. 679: Solar Wind Ten, 79–82

Sheeley, N. R., Wang, Y.-M., Hawley, S. H., Brueckner, G. E., Dere, K. P., Howard, R. A., Koomen, M. J., Korendyke, C. M., Michels, D. J., Paswaters, S. E., Socker, D. G., St. Cyr, O. C., Wang, D., Lamy, P. L., Llebaria, A., Schwenn, R., Simnett, G. M., Plunkett, S., & Biesecker, D. A. 1997, ApJ, 484, 472

Snodgrass, H. B. 1983, ApJ, 270, 288

Strachan, L., Suleiman, R., Panasyuk, A. V., Biesecker, D. A., & Kohl, J. L. 2002, ApJ, 571, 1008

Tang, F. 1981, Sol. Phys., 69, 399

Tappin, S. J., Simnett, G. M., & Lyons, M. A. 1999, A&A, 350, 302

Timothy, A. F., Krieger, A. S., & Vaiana, G. S. 1975, Sol. Phys., 42, 135

Wang, Y.-M., Hawley, S. H., & Sheeley, N. R. 1996, Science, 271, 464

Wang, Y.-M., & Sheeley, N. R. 1990, ApJ, 355, 726

Wimmer-Schweingruber, R. F., von Steiger, R., & Paerli, R. 1997, J. Geophys. Res., 102, 17407

Withbroe, G. L., & Wang, Y. 1972, Sol. Phys., 27, 394

Woo, R., & Gazis, P. R. 1994, Geophys. Res. Lett., 21, 1101

Zirin, H. 1988, Astrophysics of the Sun (Cambridge and New York, Cambridge University Press)

Zurbuchen, T. H., Fisk, L. A., Gloeckler, G., & Schwadron, N. A. 1998, Space Science Reviews, 85, 397

Zurbuchen, T. H., Fisk, L. A., Gloeckler, G., & von Steiger, R. 2002, Geophys. Res. Lett., 29, 66

Zurbuchen, T. H., Hefti, S., Fisk, L. A., Gloeckler, G., & von Steiger, R. 1999, Space Science Reviews, 87, 353

This manuscript was prepared with the AAS LaTeX macros v5.2.

Fig. 1.— A sequence of projections showing the evolution of the radial component of the magnetic field during the simulation. The abscissæ axis has the solar longitude and the ordinates axis has the latitude. The time of each frame is measured in terms of fractional solar rotations.

Fig. 2.— A sequence of projections showing the evolution of coronal holes boundaries during the simulation. The interval between the frames is the same as in Fig. 1. Dark grey areas are closed field regions and those in light grey have open magnetic field. The dots represent field line launch points that are advected by the shearing flow. Red launch points are associated with field lines that are initially closed; their color is changed to blue when the lines open up. Black launch points are associated with field lines that are initially open; their color is changed successively to green, cyan, and yellow as they close down, open up again, and close down for a second time, respectively. A black point has been enclosed by a circle to facilitate recognition as it moves into the closed field region and then out of it, changing color after it crosses each boundary. Similarly, a red point, which moves out of the closed field region into the northern coronal hole, has been enclosed in a box.

Fig. 3.— A sequence showing the evolution of magnetic field lines during the simulation. The interval between the frames is the same as in Fig. 1 and the field-line launch point correspond to those shown in Fig. 2. They are color coded according to the same scheme.

Fig. 4.— Schematic showing three possible reconfigurations of coronal fields. (a) A closed loop expands out into the solar wind. The footpoints remain anchored to the Sun. (b) Two open field lines reconnect. (c) Interchange reconnection. An open field line reconnects with a closed field line, producing a new closed and new open field line (after Crooker et al. 2002). The dashed line indicates the outer boundary.

Fig. 5.— Reconnection events occurring during the simulation and serving as examples of the three types illustrated in Fig. 4. The time separation between frames is $t_2 - t_1 = 0.0625$ solar

rotation. (a) opening up of closed field lines; (b) reconnection of open field lines that form a loop; (c) interchange reconnection between closed and open field lines. The solar surface is color coded according to the magnetic flux (red: positive flux, blue: negative flux).

Fig. 6.— A projection of the solar surface showing a coronal hole map at the time of the reconnection events of Fig. 5. Light grey areas are filled with open magnetic flux. Dark grey areas indicate the closed field regions around the equator. Regions of changing connectivity are in blue and red. Blue areas show where the magnetic field has just opened up. Conversely, the magnetic field has just closed down in red areas. Substructures are due to resolution limitations.

Fig. 7.— A sequence of projections showing the connectivity of field lines at 30 $R_{\odot}$ during the simulation. The interval between the frames is the same as as in Fig. 1. Dark regions are occupied by magnetic field lines that are connected to the solar surface. Light regions are disconnected from the solar surface.

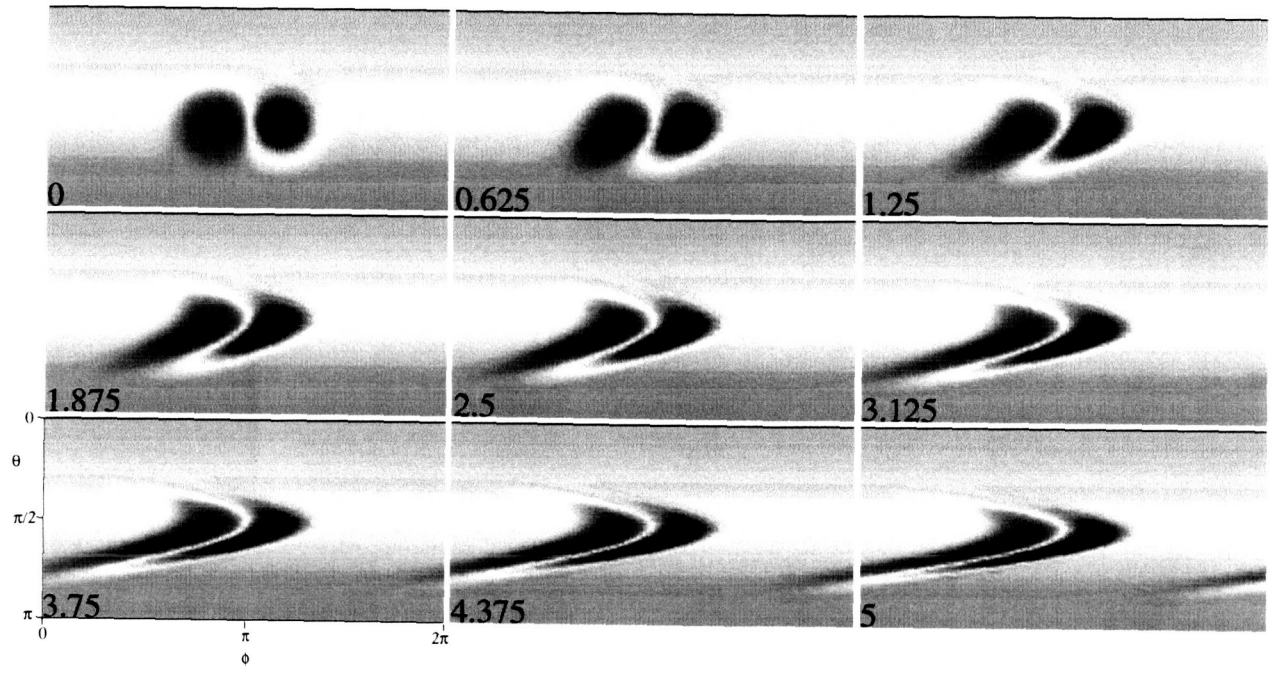

Fig. 1.—

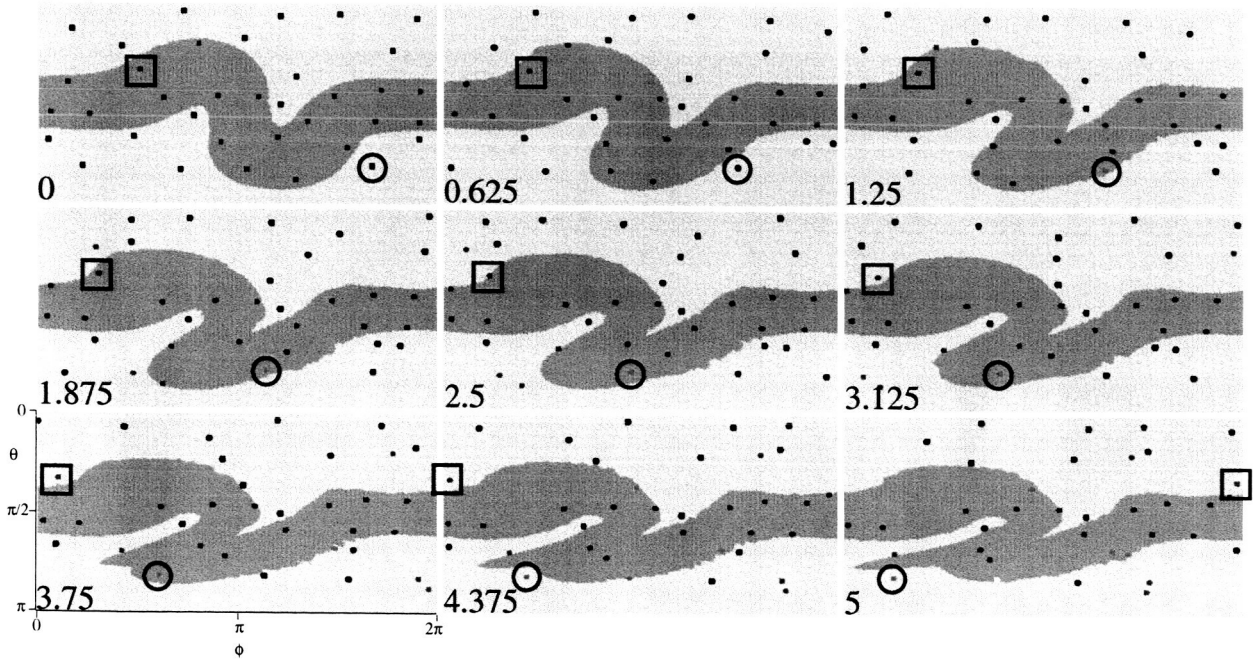

Fig. 2.—

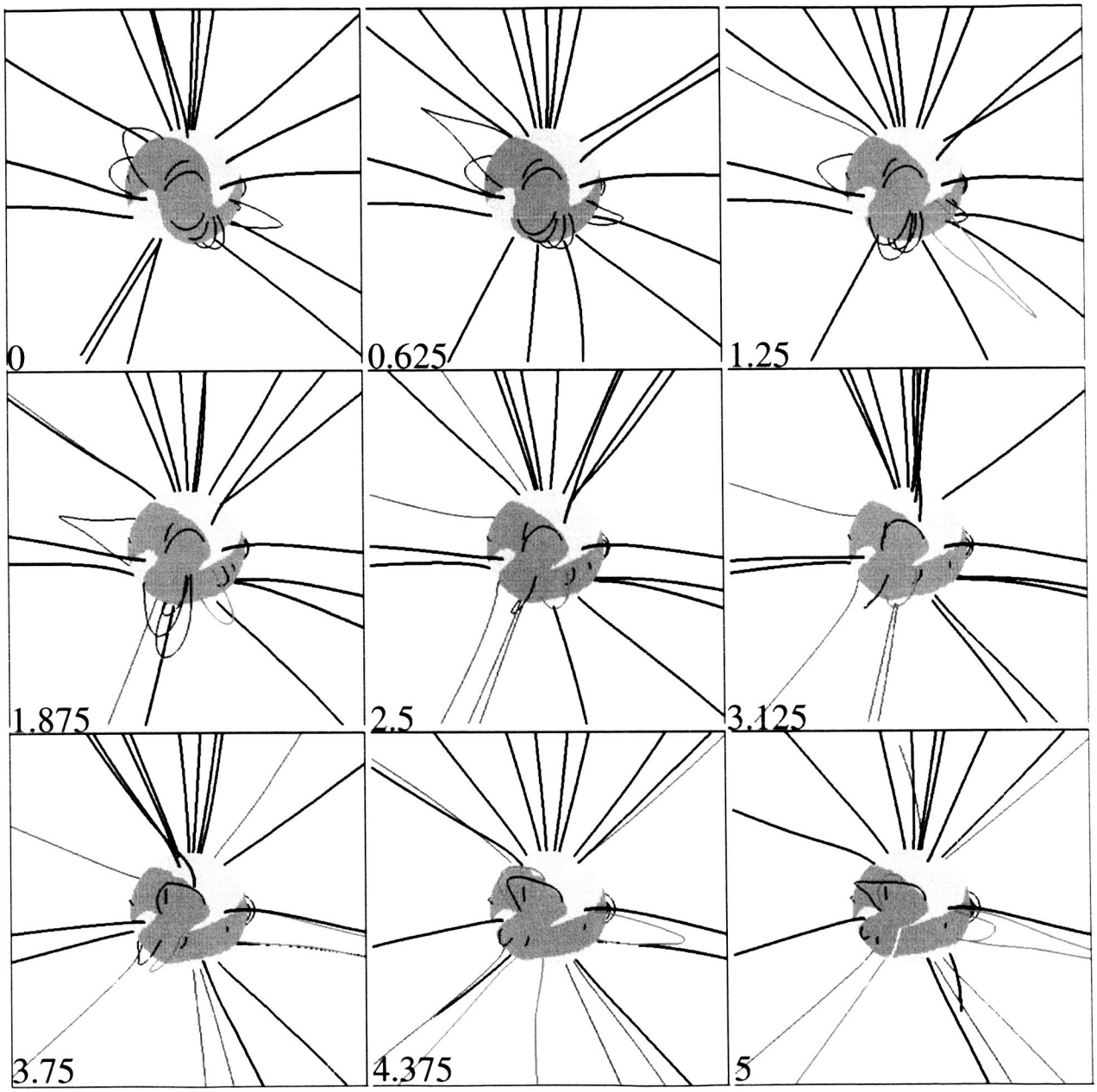

Fig. 3.—

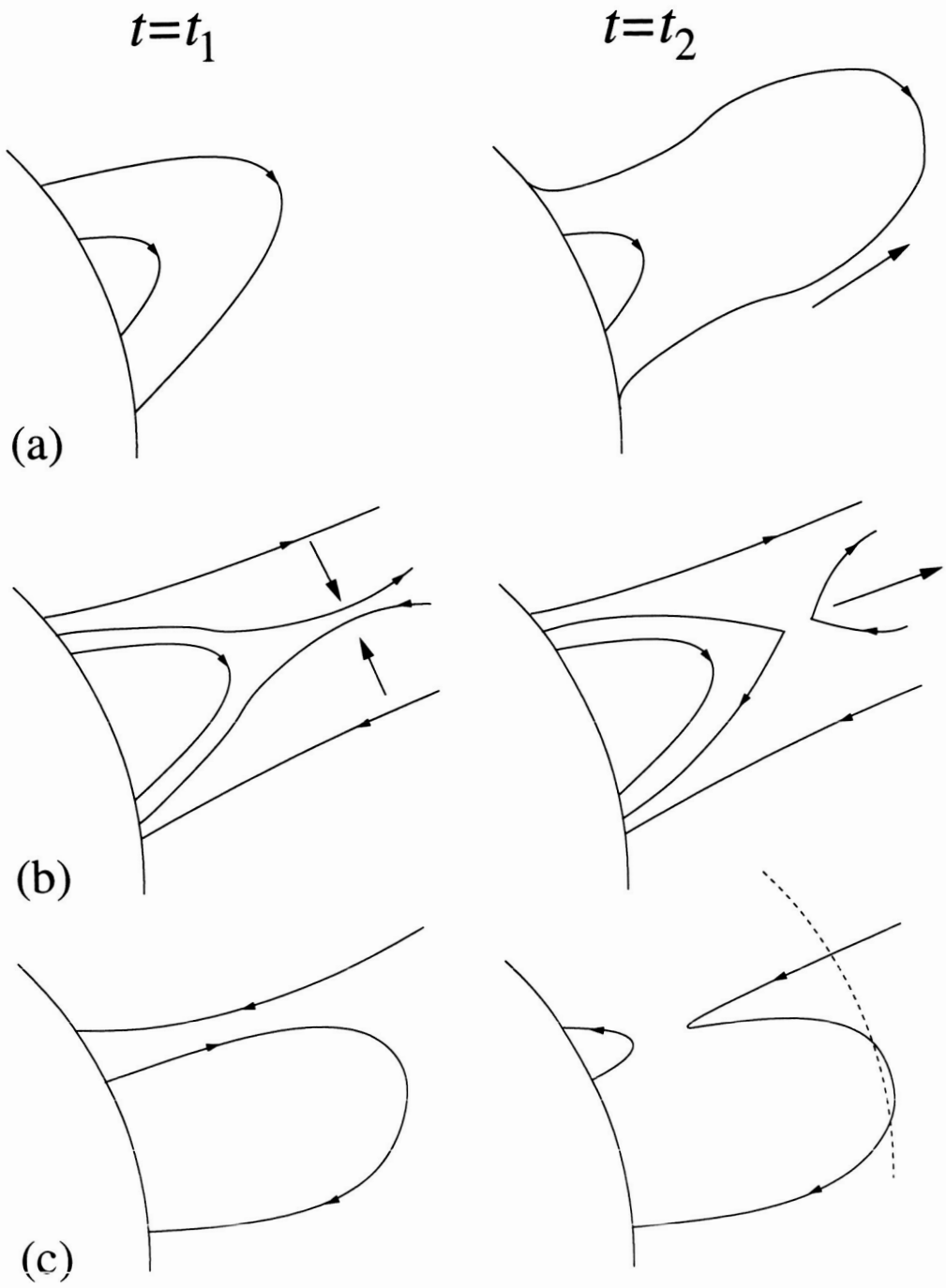

Fig. 4.—

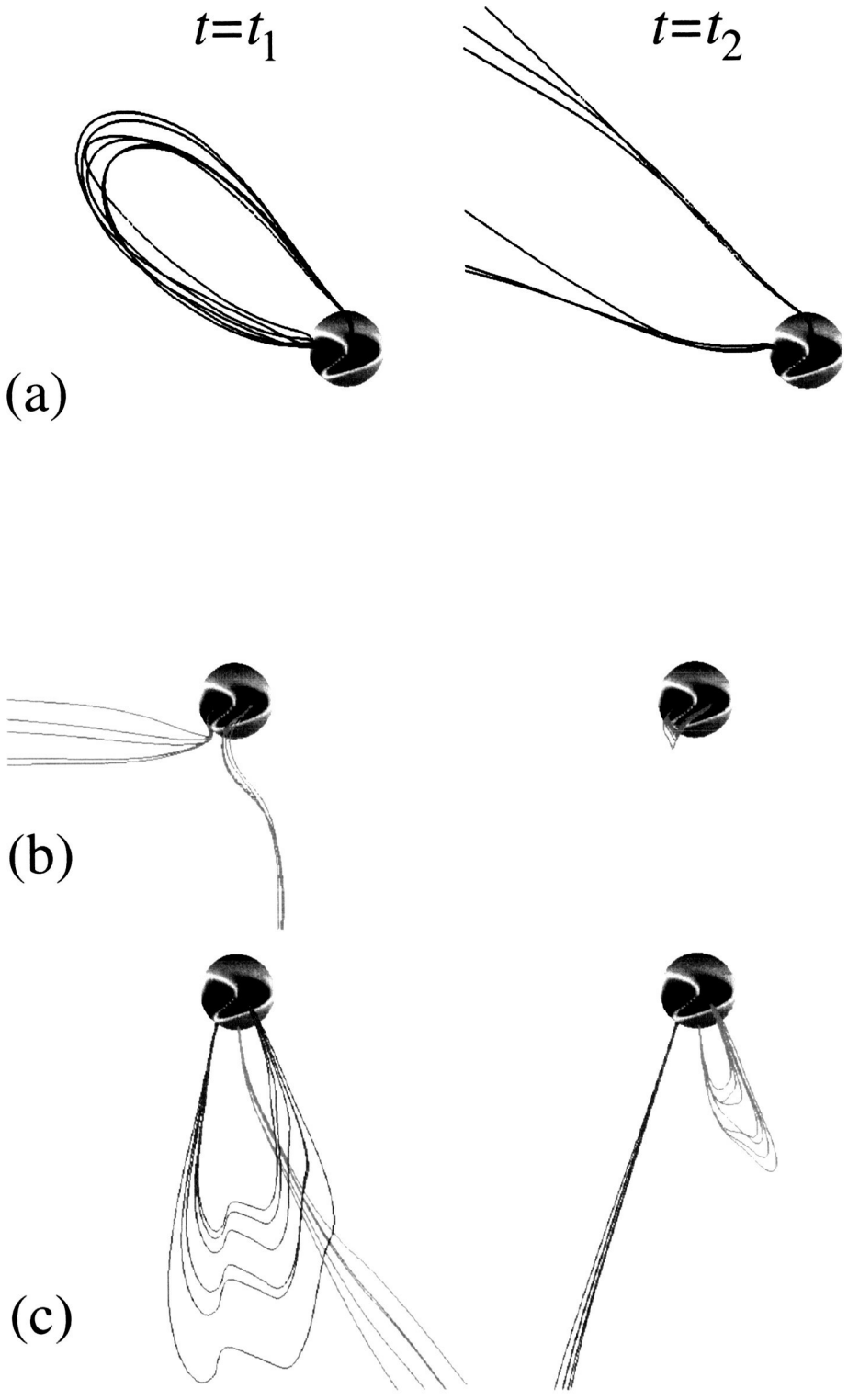

Fig. 5.—

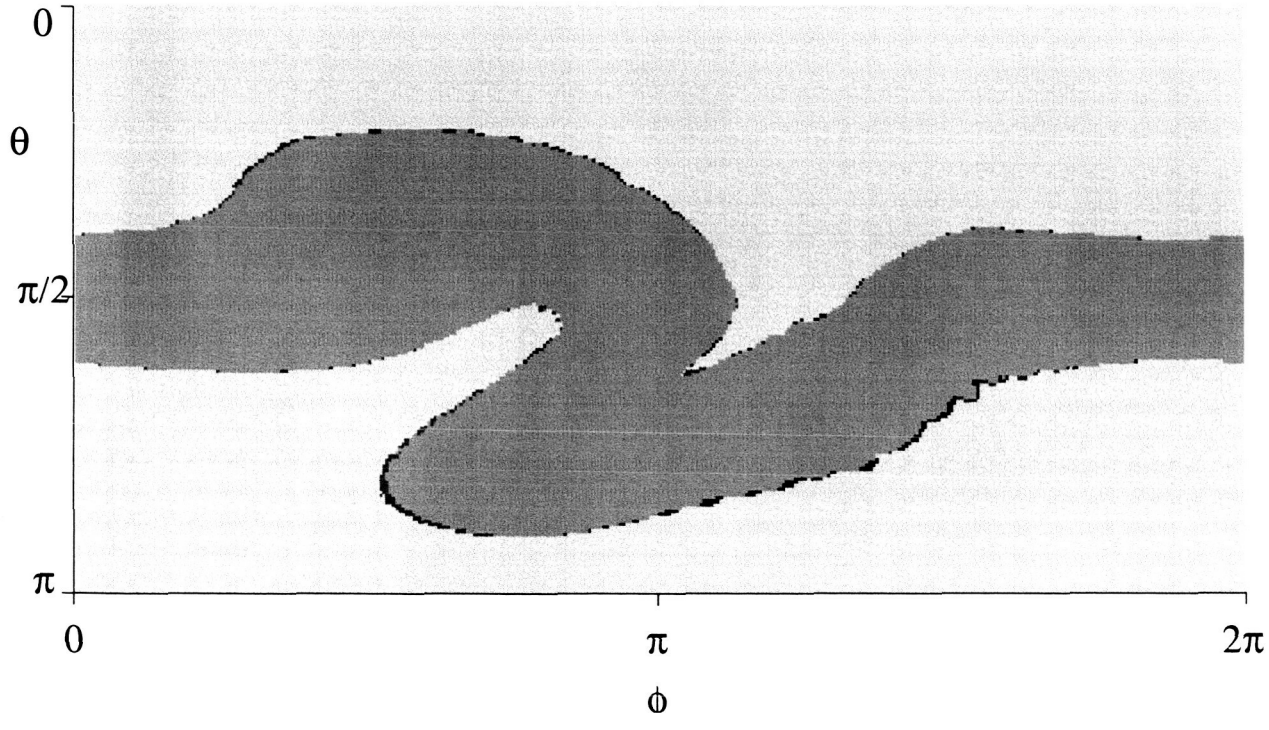

Fig. 6.—

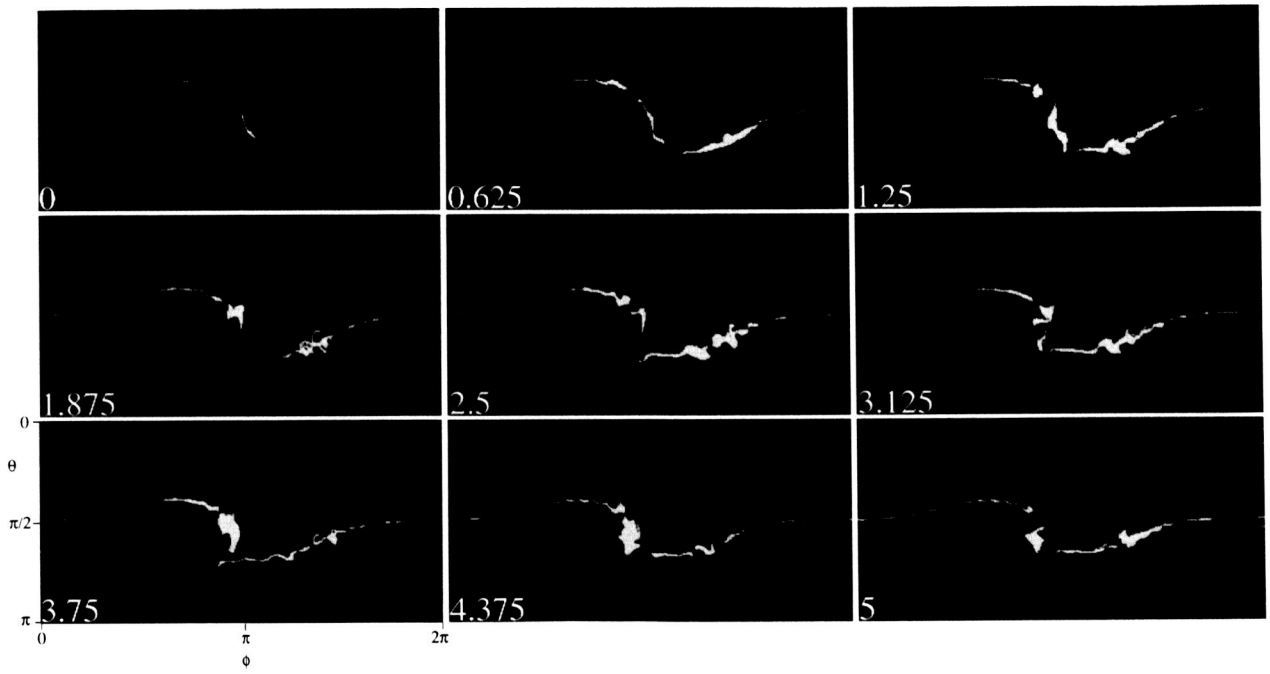

Fig. 7.—